Journal of
Materials Chemistry A

Accepted Manuscript

This is an *Accepted Manuscript*, which has been through the RSC Publishing peer review process and has been accepted for publication.

Accepted Manuscripts are published online shortly after acceptance, which is prior to technical editing, formatting and proof reading. This free service from RSC Publishing allows authors to make their results available to the community, in citable form, before publication of the edited article. This *Accepted Manuscript* will be replaced by the edited and formatted *Advance Article* as soon as this is available.

To cite this manuscript please use its permanent Digital Object Identifier (DOI®), which is identical for all formats of publication.

More information about *Accepted Manuscripts* can be found in the **Information for Authors**.

Please note that technical editing may introduce minor changes to the text and/or graphics contained in the manuscript submitted by the author(s) which may alter content, and that the standard **Terms & Conditions** and the **ethical guidelines** that apply to the journal are still applicable. In no event shall the RSC be held responsible for any errors or omissions in these *Accepted Manuscript* manuscripts or any consequences arising from the use of any information contained in them.

Table of contents entry

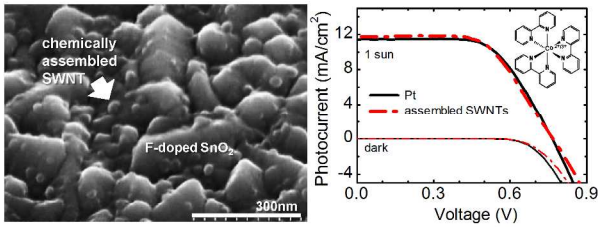

High optoelectrochemical and photovoltaic performances were achieved in $Co^{II/III}$-mediated DSCs using a carbon nanotube electrocatalyst with a loading of <5 μg/cm^2.

Journal Name

RSCPublishing

PAPER

High electrocatalytic activity of low-loaded transparent carbon nanotube assemblies for $Co^{II/III}$-mediated dye-sensitized solar cells†

Seon Hee Seo,[*a] Mi Hyung Kim,[a] Eun Ji Jeong,[ab] Sung Hwan Yoon,[a] Hyon Chol Kang,[b] Seung I. Cha[a] and Dong Yoon Lee[a]

Cite this: DOI: 10.1039/x0xx00000x

Received 30th August 2013,
Accepted

DOI: 10.1039/x0xx00000x

www.rsc.org/ees

The development of low-loaded electrocatalysts that can act as alternatives to platinum has been a long standing challenge for use in energy-related devices. Here we report that ultrashort carbon nanotube assemblies with a loading of <5 μg/cm^2 exhibits notably high optoelectrochemical and photovoltaic performances, similar to those of conventional platinum, in dye-sensitized solar cells (DSCs) employing the redox mediator cobalt(II/III)tris(2,2'-bipyridine). The electrochemical activity of the densely packed open-end-rich nanotube assemblies is strongly influenced by the redox-active species used in the organic electrolyte. The extremely high transparency (~97.5%) of the assembly allowed us to successfully fabricate $Co^{II/III}$-mediated bifacial DSCs. The power conversion efficiencies for front- and rear-side irradiation were ~4.7% and were almost insensitive to which face of the cell was irradiated.

Introduction

Dye-sensitized solar cells (DSCs) have attracted attention as low-cost alternatives to inorganic silicon solar cells.[1] A conventional DSC is a sandwich-type electrochemical cell composed of a photoactive anode, an electrolyte, and a counter electrode (CE) and irradiated from the photo-anode side. The electrolyte contains a redox mediator dissolved in an organic solvent; the mediator is responsible for regenerating the photo-oxidized dye and shuttling charge between the electrodes. The iodide/tri-iodide (I^-/I_3^-) redox mediator has been widely used as a redox mediator, but its drawbacks, such as its low electrochemical potential, high visible-light absorption and high corrosiveness,[2,3] have necessitated the development of iodine-free redox mediators.[4–7] In particular, cobalt polypyridyl redox mediators have being received considerable attention as they do not exhibit the previously mentioned disadvantages.[8,9] In order to achieve high power conversion efficiencies (η) in iodine-free DSCs, it is imperative not only to use a matched photo-sensitizer, but it is also necessary to optimize the mesoporous TiO_2 photo-anode generally used in the devices.[10,11]

In DSCs, the CE is responsible for completing the electrical circuit of the solar cell by transferring electrons from the exterior to the redox electrolyte. The electron transfer occurs at the CE/electrolyte interface toward the redox mediators. Platinum has been widely used as a CE since it exhibits good electrocatalytic activity and electrical conductivity even at thicknesses as low as a few nanometres.[12] Nevertheless, there is a strong demand for low-cost non-noble-metal electrocatalysts for industrial applications.[13] A variety of alternatives, such as conductive polymers,[14,15] metal compounds,[16] and nanocarbon materials,[17–19] have been suggested. However, most of these alternative CEs need to have a thick and porous structure in order to have high surface areas. The development of Pt-free electrodes that exhibit high electroactivity at minimum loading has been a challenging goal for use in energy-related devices. Such electrodes can decrease production costs and also increase the applicability of DSCs. For example, low-loaded transparent CEs can be used in transparent building-integrated photovoltaics[20] and in high-performance flexible DSCs based on non-transparent photo-anode on metal foil substrates.[21]

There have been two approaches to enhancing the electrochemical performance of an electrode: maximizing its electroactive surface area and increasing the electrical conductivity of the electrode. Highly conductive one-dimensional carbon nanotubes (CNTs) could be an ideal electrode material, satisfying both of these requirements. However, two-dimensional CNT electrodes usually consist of randomly distributed networks of CNTs on supporting substrates when they are fabricated by cost-effective wet coating methods.[22] Therefore, numerous junctions are inevitably present between the CNTs and at the CNT/substrate interface. Vertically aligned, long CNT mats prepared by vapour deposition methods have been proposed to decrease the

number of inefficient junction sites. However, the optimum thickness of these porous mats is still a few micrometres when they are used in DSCs.[23,24] This suggestes two possible reasons for the low specific electrochemical activity of CNT mats on conducting F-doped tin oxide (FTO): slow electron transfer at the CNT/electrolyte interface toward the redox mediators and the high junction resistance at the CNT/FTO interface. CNT mats have high sidewall-area-to-end-tip-area ratios, but there is consensus that the electrochemical activity of the basal sp^2 plane (the sidewalls of CNTs) is substantially inferior to that of edge-plane-like defects (the open ends of CNTs).[25,26] In addition, such CNT mats adhere to FTO weakly via hydrophobic interactions, but electron transfer occurs more rapidly through junctions containing chemical bonds than through junctions containing van der Waals bonds.[27,28]

The chemical assembly of CNTs on desired substrates could be an attractive method for fabricating electrodes with high electrochemical activities. However, most previous studies have been focused on performances of CNT assemblies in aqueous media for use in sensors, and such electrodes have not yet been used as an CE in DSCs.[29–31] In this study, we prepared short carboxyl-functionalized single-walled carbon nanotubes (SWNTs) on amine-terminated FTO substrates by using a self-assembly method. The chemically assembled SWNTs (ca-SWNTs) had a height of <40 nm at a loading of <5 μg/cm^2 and exhibited high electrocatalytic performances (low interfacial charge-transfer resistance and high charge-transfer rate) similar to those of a Pt analogue for the cobalt(II/III)tris(2,2'-bipyridine) ($Co(bpy)_3^{2+/3+}$) redox reaction. The high transparency (>97%) of the electrode allowed us to successfully fabricate $Co(bpy)_3^{2+/3+}$-mediated bifacial DSCs as a transparent CE.

Experimental

Preparation of SWNT electrode

SWNTs in powder form (P2, Nanocarbon Solutions) were shortened and functionalized according to the procedure reported by Liu et al.[29] In brief, 0.1 g of the P2 powder was added to 100 ml of a 3:1 mixture of concentrated sulphuric and nitric acid and sonicated for 10 h in an ice bath. The mixture was diluted with distilled water and then allowed to rest for 24 h in order to separate any carbonaceous impurities. The sediment was collected by vacuum filtration on a polycarbonate membrane filter with a pore size of 0.2 μm and washed with water until the pH of the filtrate became greater than 6.0. After being dried, 6 mg of the shortened SWNTs was dispersed in 30 mL of anhydrous dimethylsulfoxide (0.2 mg/mL). The physical and chemical properties of the pristine and the thus-prepared shortened SWNTs are summarized in Fig. S1.†

FTO glasses (15 Ω/□, Hartford) and Si<100> wafers were used as the substrates. In order to prepare the amine-terminated substrates, the substrates were first functionalized with hydroxyl groups in a piranha solution (H_2SO_4/H_2O_2=3/1, v/v) for 30 min. After being washed with water and dried with N_2, the substrates were immersed in a (3-aminopropyl) triethoxysilane (APTES, Aldrich) solution (5 mM in acetone/water =5/1, v/v) for 30 min. For the chemical assembly of the shortened SWNTs, the modified substrates were soaked in the prepared SWNT solution with 9 mg of *N,N'*-dicyclohexylcarbodiimide (DCC, Aldrich) at 40 °C for 1–21 h. The fabrication procedure of the ca-SWNT electrodes is summarized in Fig. S2.† After the completion of the reaction, the ca-SWNT electrodes were washed in acetone for 60 s under ultrasonic agitation in order to remove physisorbed CNTs. Finally, the electrodes were annealed at 300 °C in air to remove organic contaminations.

Preparation of dye-sensitized solar cells

To fabricate the photo-anodes for the DSCs, mesoporous TiO_2 layers were prepared by the procedure explained in Electronic Supplementary Information.† The prepared TiO_2 photo-anodes were soaked in a dye solution containing 0.3 mM MK-2 (2-cyano-3-[5‴-(9-ethyl-9*H*-carbazol-3-yl)-3′,3″,3‴,4-tetra-*n*-hexyl-[2,2′,5′,2″,5″,2‴]-quater thiophen-5-yl] acrylic acid, Aldrich) dye in toluene and left overnight. The stained TiO_2 working electrodes were assembled with the prepared ca-SWNT or thermally platinised FTO CE along with a 25-μm-thick Surlyn gasket (Meltronix 1170-25, Solaronix). The electrolyte was injected by vacuum back filling through a hole on the counter electrode in a dry room. The $Co(bpy)_3^{2+/3+}$ redox mediators, $[Co(bpy)_3](PF_6)_2$ and its oxidized form $[Co(bpy)_3](PF_6)_3$, were synthesized as reported previously.[9] The composition of the electrolyte was 0.165 M $[Co(bpy)_3](PF_6)_2$, 0.045 M $[Co(bpy)_3](PF_6)_3$, 0.1 M $LiClO_4$ (Aldrich), and 0.2 M 4-*tert*-butylpyridine (Aldrich) in acetonitrile. To form stable electrical contacts between the cells and the external circuit, the edges of the FTO glasses were ultrasonically soldered with metal wires (MBR Electronics GmbH, Cerasolzer, Alloy #CS186) for all the measurements.

Measurements

Field-emission scanning electron microscopy (FE-SEM) and atomic force microscopy (AFM) were performed using a Hitachi S4800 system and a XE-100 system (Park System) in the non-contact mode, respectively. The ca-SWNT electrodes were subjected to micro-Raman spectroscopy using 532 nm and 633 nm lasers (NT-MDT, NTEGRA SPECTRA). Ultraviolet-visible (UV-vis) spectroscopy was performed using a Cary 5000 spectrophotometer (Varian). The photocurrent–voltage (*J–V*) characteristics were determined using a Keithley model 2400 source measurement unit. The irradiation source was a 300 W Xenon lamp on an Oriel solar simulator with an air mass 1.5G filter. In order to eliminate the diffuse scattering from the edges of the glass substrates during the photovoltaic *J–V* measurements, black masks smaller than the printed TiO_2 area were attached on the surfaces of the DSCs, and the active area was defined to 0.2025 cm^2. In case of the transparent bifacial DSCs, black masks slightly larger than the photoactive area

were used to prevent inaccurate irradiation from the rear-side, and the active area was defined to 0.250 cm^2.

The electrochemical characterizations were performed using a BioLogic SP-300 potentiostat. Electrochemical impedance spectroscopy (EIS) was performed and the Tafel polarizations were measured using symmetrical closed dummy cells with two identical electrodes. The impedance spectra were acquired under open-circuit conditions. The modulation amplitude was 10 mV and frequency range was 0.3 Hz to 10^5 Hz. The EIS data were processed using the ZSimpWin software. Cyclic voltammetry (CV) was performed using a three-electrode setup. The electrolyte used was an acetonitrile solution containing 2 mM $[Co(bpy)_3](PF_6)_2$ and 0.1 M tetrabutylammonium hexafluorophosphate ($TBA{\cdot}PF_6$). A Pt plate and a Ag/Ag^+ reference electrode (10 mM $AgNO_3$ and 0.1 M $TBA{\cdot}PF_6$ in acetonitrile) were used as the counter and the reference electrodes, respectively.

Results and discussion

Prior to the chemical assembly of the carboxyl-functionalized SWNTs[27] (Fig. S1†) on rough FTO substrates, SWNTs were first assembled on smooth Si wafers modified with hydroxyl and amine groups in the presence of a coupling agent, DCC.[32,33] The pre-treated substrates were prepared by piranha treatment and via self-assembly using APTES, respectively. The carboxyl ends of the shortened SWNTs transformed into ester links on the hydroxyl-terminated substrates (OH/substrate) or formed an amide bond on the APTES-modified amine-terminated substrates (APTES/substrate) after the DCC reaction.[34,35] The AFM images in Fig. 1a–b show clearly the assembly of short SWNTs (ca-SWNT) on the modified substrates after a reaction period of 1 h. It can also be seen that the density of the SWNT assembly on the APTES/Si substrate was greater than that on the OH/Si substrate early in the assembly process. A negatively charged SWNT with a carboxyl group binds more readily to the protonated amine group than to the negatively charged hydroxyl group.

The electrochemical performances of the ca-SWNTs were studied using CV. The ca-SWNT electrodes were prepared on both OH/FTO and APTES/FTO substrates under preparation conditions similar to those used for Si-based ones. Fig. 1c shows the CV curves obtained for 2 mM $[Co(bpy)_3](PF_6)_2$ in acetonitrile with 0.1 M $TBA{\cdot}PF_6$ using a three-electrode configuration at the scan rate of 100 mV/s. A cathodic material catalyzes the oxidized form of the redox mediator into the reduced form. Thus, the CV curves can be characterized using the cathodic peak current ($I_{p,c}$) and the peak-to-peak separation potential (ΔE_{pp}).[36] Under a given measurement condition, the higher the $I_{p,c}$, the larger the electroactive surface area. A decrease in ΔE_{pp} corresponds to relatively higher rates of electron transfer at the electrode/electrolyte interface. As shown in Fig. 1c, bare and modified FTO substrates without the ca-SWNTs showed only small cathodic peaks at approximately –0.15 V, indicating poor electrochemistry at the corresponding

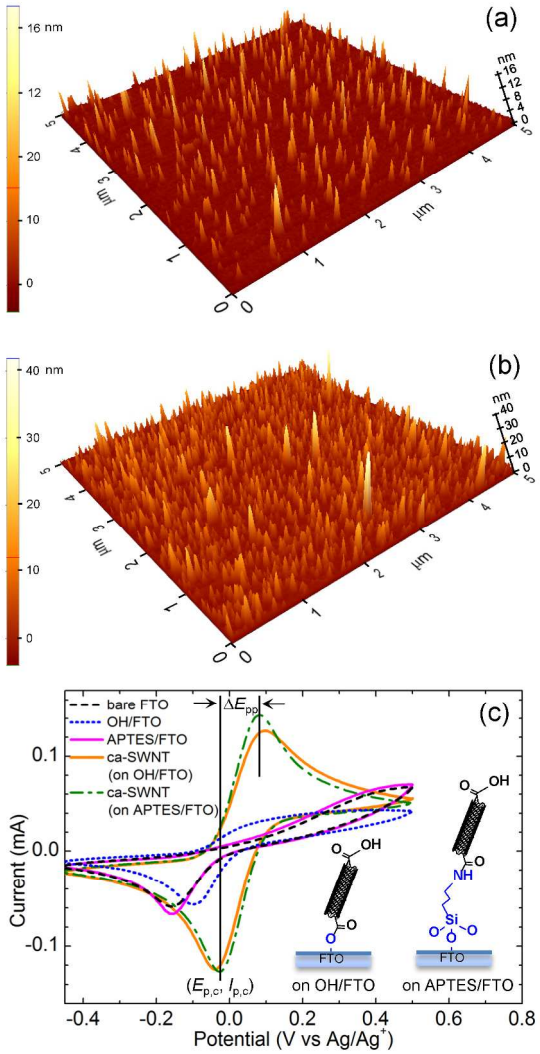

Fig. 1 AFM images of ca-SWNT assemblies formed from the shortened SWNTs on (a) hydroxyl- (OH/Si) and (b) APTES-modified Si (APTES/Si) substrates after the DCC reaction for 1 h. (c) Cyclic voltammograms for 2 mM $[Co(bpy)_3](PF_6)_2$ in acetonitrile with 0.1 M $TBA{\cdot}PF_6$ electrolyte at the scan rate of 100 mV/s. The insets show schematic illustrations of the ca-SWNTs bonded on each substrate.

interfaces.

After the OH/FTO and APTES/FTO substrates had been immersed in a solution of shortened SWNTs for 1 h, the larger $I_{p,c}$ and the appearance of a pair of distinctive peaks suggested that facile electrochemistry occurred at the ca-SWNT electrodes (Fig. 1c). The SWNTs were assembled on the OH/FTO substrate in a much lower density (Fig. 1a), resulting in larger ΔE_{pp} and only slightly lower $I_{p,c}$ than those for the SWNTs on the APTES/FTO substrate. From the measured values of $I_{p,c}$, the electroactive surface areas of the ca-SWNTs were estimated to be 0.348 and 0.361 cm^2 on the OH/FTO and the APTES/FTO substrates, respectively (see ESI† for detailed calculation). These values are not much different from each other and are in contrast to what can be expected from the AFM images. The apparent ΔE_{pp} decreased from ~134 to ~109 mV on changing the link layer from hydroxyl to amine-terminated APTES, and quasi-reversible electrochemistry occurred for the

$Co(bpy)_3^{2+/3+}$ redox reaction. The CV results indicate clearly that the APTES link layer accelerated electron transfer rather than enlarging the electroactive area, despite the insulating nature of APTES.

To investigate the effect of the reaction time on the structural properties of the ca-SWNTs, we prepared ca-SWNTs on APTES/Si and APTES/FTO substrates using different reaction times. Fig. 2a–d show SEM images of the ca-SWNT assemblies formed for DCC reactions of 1 h and 21 h. Owing to the low contrast between the ca-SWNTs and the substrates in top-view SEM images, we captured images from samples mounted on a 45°-tilted stage. This allowed the nanometre-scaled ca-SWNTs to be easily distinguished from the substrates. The SWNTs tended to assemble in hemispherical shapes (heights of less than ~40 nm) owing to the condensation of the adsorbed short SWNTs during the assembly process (Fig. S3†).[37] In addition, as can be seen, their size increased with the reaction time.

To verify the presence of SWNTs on each substrate, Raman spectroscopy was performed (Fig. 2e–f). SWNTs exhibit unique features in their Raman spectrum, allowing the presence of SWNTs in the ca-SWNTs to be proved.[38] The Raman spectrum of SWNTs usually has two kinds of characteristics: a radial breathing mode (RBM) and a doublet G band (at ~1570 and ~1590 cm^{-1}). The diameter of the ca-SWNTs was estimated to be ~1.49 nm using the relation $d_t \approx 248/\omega_{RBM}$, where d_t is the nanotube diameter in nanometres and ω_{RBM} is the RBM frequency,[38] obtained from Fig. 2e. The estimated diameter was close to that claimed by the manufacturer (1.4 nm). The spectra for the ca-SWNTs showed a distinct doublet G band, which provided concrete evidence that the assemblies on both substrates, shown in Fig. 2a–d, consisted of SWNTs. The disorder or D band was also present in the spectra, and the peak intensity ratio I_D/I_G was used to determine the crystallographic disorder. As the reaction time increased, the I_D/I_G ratio decreased from 0.37 to 0.12 in the case of the FTO substrates, indicating the formation of relatively longer SWNT assemblies for the longer reaction time.

The substantial changes in the surface morphologies and crystallographic properties of the ca-SWNTs with the reaction time had a slight effect on $I_{p,c}$ and the charge-transfer resistance (R_{CT}) at the ca-SWNT/electrolyte interface (6.2–7.3 Ω cm^2, see Fig. S4† and R_{CT} is discussed below). The minimal changes in the $I_{p,c}$ and the R_{CT} imply that the individual SWNTs within the assembled ca-SWNT domains were packed too tightly to allow the redox-active species to diffuse into the domains as can be expected from the cross-sectional images of Fig. S3†; this can seriously inhibit increases in the effective surface area with respect to the reaction time. This indicates that the ca-SWNT electrode had a rough nonporous structure, which was on the scale of tens of nanometres, and its outermost surface contained a number of redox-active edge-plane-like defects with oxygen functional groups. Furthermore, the electrical conductivity of

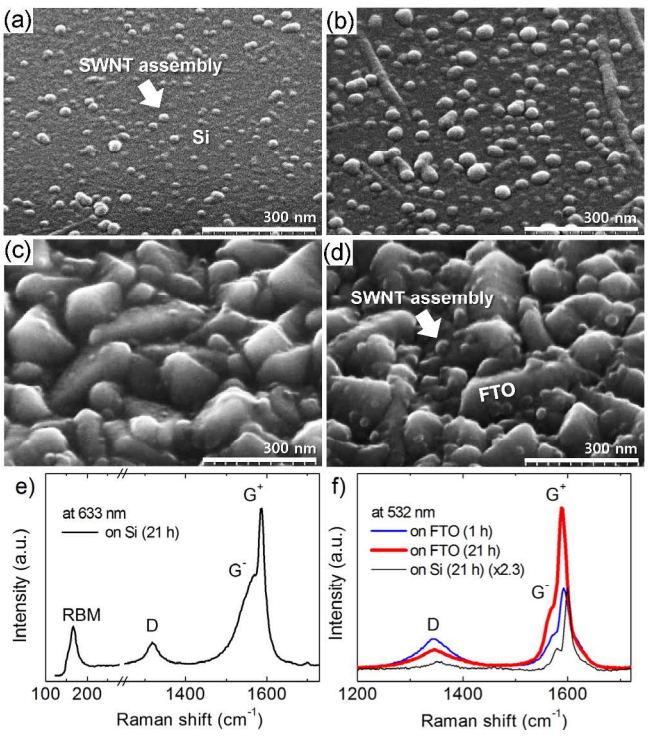

Fig. 2 Side-view SEM images of the ca-SWNTs formed on (a, b) APTES/Si and (c, d) APTES/FTO substrates. The reaction times were 1 h and 21 h, respectively. Raman spectroscopy was performed with (e) 633 nm and (f) 532 nm lasers.

the shortened SWNTs would not limit the electrochemical activity of the resulting electrode because only ultrashort SWNTs with lengths of less than 40 nm in the SWNT suspension were chemically assembled on conducting substrates. As a result, charge would be transported immediately from the conducting substrate to redox-active sites of the ca-SWNT electrode.

To examine the feasibility of using the ca-SWNTs as an electrocatalyst in practical applications, we used the ca-SWNT electrode as a CE in DSCs employing the $Co(bpy)_3^{2+/3+}$ redox mediator and studied the photovoltaic and electrochemical characteristics of the DSCs in detail (Fig. 3). The power conversion efficiency (η) of a solar cell is defined as the ratio of the maximum power ($J_m \times V_m$) as determined from the photovoltaic J–V curve to the irradiated light power (100 mW/cm^2, 1 sun in this work). The other relevant parameters are the short-circuit current density (J_{SC}) at V=0, the open-circuit voltage (V_{OC}) at net zero current, and the fill factor (FF) corresponding to the "squareness" of the J–V curve defined by $(J_m \times V_m)/(J_{SC} \times V_{OC})$.[39] The electrochemical performance of the CE mainly affects the FF, but sometimes also decreases the J_{SC} if the exchange current density at the CE/electrolyte interface is lower than that required at an opposite oxidized photo-anode. $Co^{II/III}$-mediated DSCs using commercialized MK-2 organic dye have exhibited an η of 5.5–6.5%.[24,40] Thus, using this dye makes a readily accessible system for investigating the performances of the components used in $Co^{II/III}$-mediated DSCs.

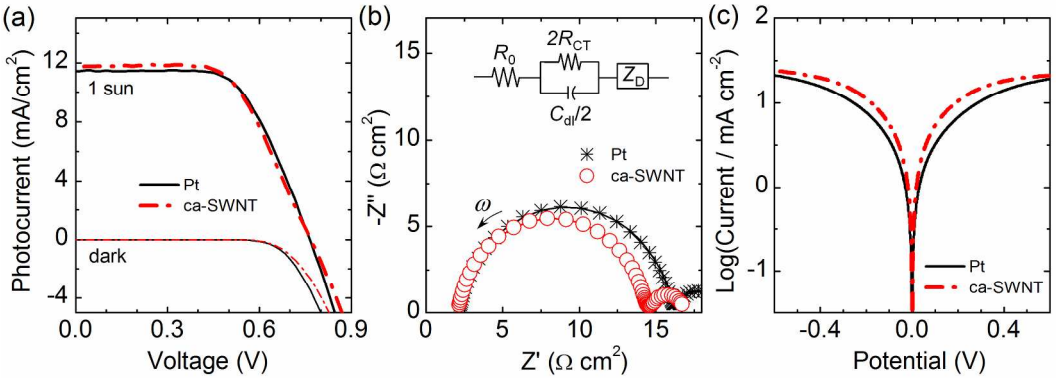

Fig. 3 (a) Photovoltaic *J*–*V* curves of Co(bpy)$_3^{2+/3+}$-mediated DSCs with the ca-SWNT or Pt CEs under simulated light (100 mW/cm^2, 1 sun) and in the dark. (b) The Nyquist plot of the EIS data obtained under an open-circuit condition using symmetrical closed dummy cells. The inset shows the corresponding equivalent circuit. (c) The Tafel polarization curves of the dummy cells used for the EIS measurements.

In this work, a MK-2-sensitized solar cell with the ca-SWNT CE exhibited good photovoltaic performance, with an V_{OC} of ~0.767 V, J_{SC} of ~11.75 mA/cm^2, FF of ~0.607, and η of 5.47%; these values were similar to those obtained using a conventional Pt CE (V_{OC} of ~0.764 V, J_{SC} of ~11.44 mA/cm^2, FF of ~0.627, and η of 5.48%, Fig. 3a). The obatined V_{OC} were lower than reported values of Co(bpy)$_3^{2+/3+}$-mediated DSCs (>0.9).[9,11] This might attribute to the small steric barrier group in the MK-2 dye structure and then the fast back electron transfer from the TiO_2 surface to the oxidized Co(bpy)$_3^{3+}$,[40] which induces a band edge shift at the TiO_2 surface toward more positive potential[41] and then a smaller difference between the band edge and the redox potential of Co(bpy)$_3^{2+/3+}$, directly correlated to V_{OC}.

Fig. 3b shows the Nyquist plot of the EIS data obtained using symmetrical closed dummy cells consisting of either two identical ca-SWNTs or Pt electrodes. The geometrical configuration and the electrolyte used were the same as those in the DSCs. An interfacial R_{CT} can be estimated by fitting the EIS data using symmetrical dummy cells on the basis of a well-established equivalent circuit[42] as shown in the inset of Fig. 3b. In this work, R_{CT} roughly corresponds to the radius of a semicircle at a higher frequency in the Nyquist plot (see ESI† for detailed calculation). The R_{CT} of the ca-SWNT was 6.2 Ω cm^2 and similar to that of the Pt one (6.4 Ω cm^2). Moreover, the effective double-layer capacitances (C_{dl}) of the ca-SWNT and the Pt CEs were estimated to be 8.8 and 10.6 μF/cm^2, respectively, in the Co(bpy)$_3^{2+/3+}$ redox electrolyte (see ESI† for detailed calculation). Considering that C_{dl} is proportional to the effective surface area, it should be noted that even though the ca-SWNT electrode had a small electroactive surface area, in contrast to those of previously reported thick and porous nanocarbon-based CEs,[17–19,23] it exhibited good electrochemistry comparable to that of the Pt electrode with respect to the Co(bpy)$_3^{2+/3+}$ redox reaction. We could estimate the level of SWNT loading in the ca-SWNT electrode on the basis of the density of the closely packed SWNT assemblies (1.2 g/cm^3, a saturated value after the reaction of 2 h).[43] If one assume that the densely packed SWNT assembly was formed in a thin layer with heights of 20–40 nm (Fig. S3†), the estimated loading rates become 2.4–4.8 μg/cm^2; those are lower than 5 μg/cm^3, which is the lowest reported in the case of nanocarbon-based electrodes with high electrocatalytic activity.

The electrochemical activity of the ca-SWNTs showed a strong dependence on the redox mediator. The ca-SWNT electrodes exhibited poor electrochemistry with respect to the conventional I^-/I_3^- redox reaction, which resulted in the S-shaped *J*–*V* curve of the iodine-based DSCs with the substantially low FF (Fig. S5 and Table S1†). The considerable decrease of the FF with respect to the change of redox mediators might result from the reversal of electrostatic interactions between the redox mediators and the carboxylic functionalized ca-SWNTs with the small surface area. The high electrocatalytic activity of the ca-SWNT electrode, especially with respect to the Co(bpy)$_3^{2+/3+}$ redox reaction could be due to an electrostatic attraction between the negatively charged carboxyl group at the ends of the ca-SWNTs and the positively charged Co(bpy)$_3^{3+}$ redox mediator and then the attractive interaction could accelerate interfacial charge transfer.[9] As can be seen from the Bode plot of Fig. 4, the corresponding characteristic peak shifted considerably toward the higher-frequency region (from ~10 to ~2500 Hz) with respect to the redox mediator, indicating that a much faster charge transfer occurred at the interface toward the positively charged Co(bpy)$_3^{2+/3+}$ than toward the negatively charged I^-/I_3^- redox

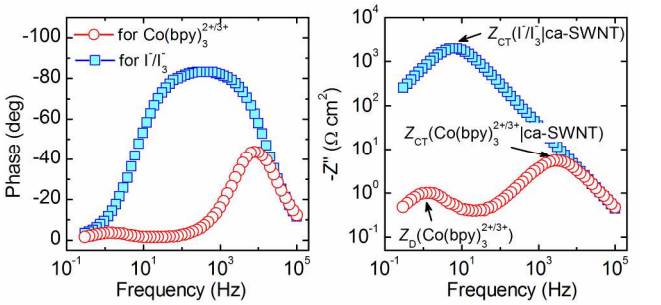

Fig. 4 Bode plots of the EIS data shown in Fig. 3 and Fig. S5† with respect to the redox electrolyte in the case of the ca-SWNT electrodes.

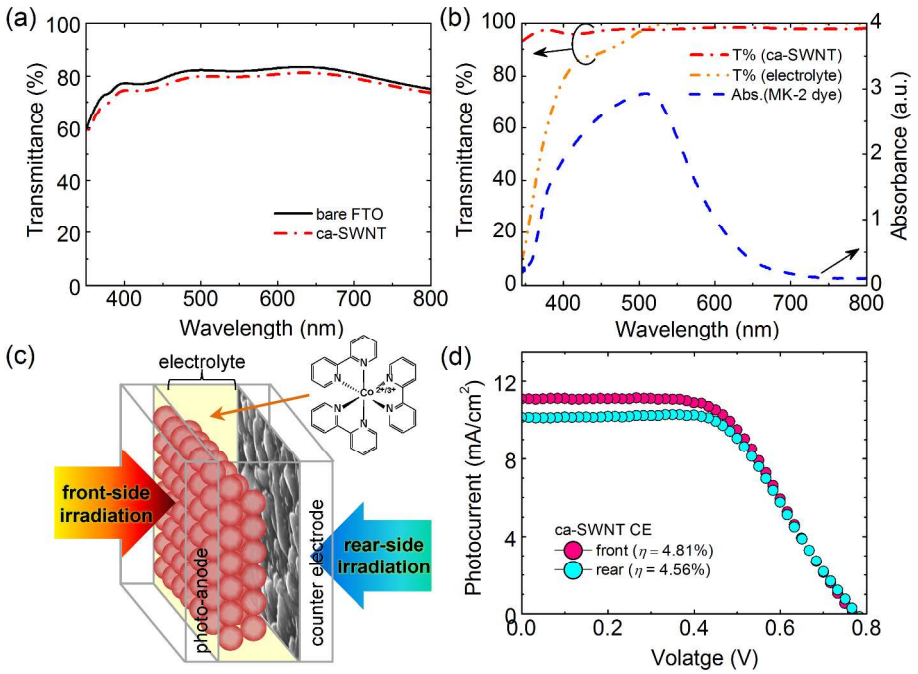

Fig. 5 (a) Transmittances of a bare FTO and the ca-SWNT electrode with respect to a baseline (air). (b) Transmittances and absorbance of the components of the DSCs with respect to the basis of FTO glass. (c) A schematic illustration of the bifacial DSC and (d) photovoltaic *J*–*V* curves of $Co(bpy)_3^{2+/3+}$-mediated bifacial DCSs with the ca-SWNT CE.

mediator. In order to compensate for the slow charge transfer in the popular I^-/I_3^- redox electrolyte, previous alternative CEs have been mostly focused on the increase of electroactive surface areas by controlling the porosity and defect density of these materials or by attaching functional groups to them[44] rather than on the increase of the charge-transfer rate. Therefore, employing a properly matched redox mediator can be a useful approach for achieving high electrocatalytic activity in low-loaded nanocarbon electrodes.

To further confirm the electrochemical performances of the ca-SWNTs, the Tafel polarization curves of the electrodes were also plotted using the symmetrical dummy cells used for the EIS measurements (Fig. 3c). The limiting current density (J_{lim}) of an electrode is influenced by the diffusion of the electroactive species in the thin-layer cell. The diffusion coefficient of $Co(bpy)_3^{3+}$ was found to be 6.42×10^{-6} cm^2/s (see ESI† for detailed calculation); this was exactly similar to that reported previously (6.4×10^{-6} cm^2/s).[45] The rapid approach to a plateau, J_{lim}, with a steeper slope indicates a higher exchange current and a somewhat higher electrochemical activity. The ca-SWNT CE, whose polarization curve had a steeper slope, exhibited as high an electrochemical activity in the $Co(bpy)_3^{2+/3+}$ redox electrolyte as can be expected.

The optical properties of the ca-SWNT electrodes were also characterized with respect to their application in transparent bifacial DSCs. When a bifacial DSC is irradiated from the CE side (rear-side), the intensity of light arriving at the TiO_2 photo-anode would depend on the transmittances of the electrocatalyst and the electrolyte layer as well as the FTO glass substrate. The transmittance of the FTO glass substrate used was 80%, averaged over the wavelength (λ) range 350–800 nm; the ca-SWNTs on a FTO glass also exhibited a noticeably high transmittance of 78% (Fig. 5a). This means the ca-SWNTs absorbed only ~2.5% of the visible light transmitted through the FTO glass over a wide range of λ in case of the rear-side irradiation. A transmittance as high as ~97.5% has never been reported for high-performance alternative CEs (Fig. 5b).[45,46] The photosensitive MK-2 dye was adsorbed on a transparent mesoporous TiO_2 layer, absorbing light from 350 to 700 nm. The layer of the $Co(bpy)_3^{2+/3+}$ redox electrolyte transmitted light for λ >340 nm (Fig. 5b), in contrast to the conventional I^-/I_3^- redox mediator with an onset λ >400 nm.[21] Therefore, as shown in Fig. 5c, MK-2-sensitized bifacial DSCs irradiated from the rear-side will benefit from the high transmittance of both the ca-SWNT CE and the $Co(bpy)_3^{2+/3+}$ redox electrolyte over a wide range of λ.

Fig. 5d shows the photovoltaic *J*–*V* curves of a bifacial DSC with a transparent ca-SWNT CE and a semitransparent TiO_2 photo-anode; the DSC was irradiated from the front and the rear sides. The change of irradiation faces obviously caused the decrease of J_{SC} due to the difference in traveling paths of incident light arriving at each side of the photo-anode layer. The DSC under rear-side irradiation exhibited a η of 4.56%, which was ~95% of the η achieved when the DSC was subjected to front-side irradiation (4.81%). This power conversion ratio is higher than that reported previously for bifacial DSCs.[14,15,20,47] The relatively small decrease in J_{SC}—this was in contrast to the previous performances of bifacial DSCs—arose from the high transparency of the ca-SWNT CE. The lower transmittance of the CE had a negative effect on the

J_{SC} of the bifacial DSCs (Fig. S6–7†); this emphasizes the importance of the transparency of the CEs used in advanced solar cells that employ rear-side irradiation.

Conclusions

In summary, we chemically assembled SWNTs (ca-SWNTs) on amine-terminated FTO glasses as novel high-performance transparent electrocatalysts and successfully used these in bifacial $Co^{II/III}$-mediated DSCs. Even though the assembled SWNTs had low loading of <5 μg/cm^2 (heights less than 40 nm), the ultrashort ca-SWNTs exhibited quasi-reversible electrochemistry especially toward the $Co(bpy)_3^{2+/3+}$ redox mediator. A normal opaque MK-2-sensitized solar cell with the ca-SWNT CE exhibited a photovoltaic power conversion efficiency (5.47%) similar to that obtained using a conventional Pt CE (5.48%). The highly electrocatalytic ca-SWNT electrode also exhibited an extremely high transmittance, of ~97.5%, averaged over the wavelength of 350–800 nm. The conversion efficiency of a transparent bifacial solar cell fabricated using the ca-SWNT electrode was as high as ~4.7% and was almost insensitive to which face of the cell was irradiated. Therefore, the thus-synthesized highly electrocatalytic SWNT assembly is a suitable low-cost substitute for expensive Pt for fabricating transparent CEs to be used in high-performance transparent or metal-foil-based flexible DSCs in combination with the appropriate redox mediators.

Acknowledgements

This work was supported by a grant from Korea Electrotechnology Research Institute.

Notes and references

[a] Nano Hybrid Technology Research Center, Korea Electrotechnology Research Institute, Changwon 641-120, Korea. E-mail: seosh@keri.re.kr; Tel: +82-55-280-1645; Fax: +82-55-280-1590
[b] Department of Advanced Materials Engineering, College of Engineering, Chosun University, Gwangju 501-759, Korea
† Electronic Supplementary Information (ESI) available. See DOI: 10.1039/b000000x/

1 B. O'Regan and M. Gratzel, *Nature*, 1991, **353**, 737–740.
2 J. N. Clifford, E. Palomares, Md. K. Nazeeruddin, M. Grätzel, and J. R. Durrant, *J. Phys. Chem. C*, 2007, **111**, 6561–6567.
3 G. Boschloo and A. Hagfeldt, *Acc. Chem. Res.*, 2009, **42**, 1819–1826.
4 S. Sapp, M. Elliott, C. Contado, S. Caramori, and C. A. Bignozzi, *J. Am. Chem. Soc.*, 2002, **124**, 11215–11222.
5 M. Wang, N. Chamberland, L. Breau, J.-E. Moser, R. Humphry-Baker, B. Marsan, S. M. Zakkeruddin, and M. Grätzel, *Nat. Chem.*, 2010, **2**, 385–389.
6 T. Daeneke, T-H. Kwon, A. B. Holmes, N. W. Duffy, U. Bach, and L. Spiccia, *Nat. Chem.*, 2011, **3**, 211–215.
7 T. W. Hamann and J. W. Ondersma, *Energy Environ. Sci.*, 2011, **4**, 370–381.
8 D. Zhou, Q. Yu, N. Cai, Y. Bai, Y. Wang, and P. Wang, *Energy Environ. Sci.*, 2011, **4**, 2030–2034.
9 S. M. Feldt, E. A. Gibson, E. Gabrielsson, L. Sun, G. Boschloo, and A. Hagfeldt, *J. Am. Chem. Soc.*, 2010, **132**, 16714–16724.
10 A. Yella, H.-W. Lee, H. N. Tsao, C. Yi, A. K. Chandiran, Md. K. Nazeeruddin, E. W.-G. Diau, C.-Y. Yeh, S. M. Zakeeruddin, and M. Grätzel, *Science*, 2011, **334**, 629–633.
11 J.-H. Yum, E. Baranoff, F. Kessler, T. Moehl, S. Ahmad, T. Bessho, A. Marchioro, E. Ghadiri, J.-E. Moser, C. Yi, Md. K. Nazeeruddin, and M. Grätzel, *Nat. Commun.*, 2012, **3**, 631
12 N. Papageorgiou, *Coord. Chem. Rev.*, 2004, **248**, 1421–1446.
13 M. Wu and T. Ma, *ChemSusChem*, 2012, **5**, 1343–1357.
14 S. Ahmad, J.-H. Yum, Z. Xianxi, M. Grätzel, H.-J. Butt, Md. K. Nazeeruddin, *J. Mater. Chem.*, 2010, **20**, 1654–1658.
15 J. Burschka, V. Brault, S. Ahmad, L. Breau, Md. K. Nazeeruddin, B. Marsan, S. M. Zakeeruddin and M. Grätzel, *Energy Environ. Sci.*, 2012, **5**, 6089–6097.
16 M. Wu, X. Lin, Y. Wang, L. Wang, W. Guo, D. Qi, X. Peng, A. Hagefeldt, M. Grätzel and T. Ma, *J. Am. Chem. Soc.*, 2012, **134**, 3419–3248.
17 S. H. Seo, S. Y. Kim, B.-K. Koo, S.-I. Cha and D. Y. Lee, *Langmuir*, 2010, **26**, 10341–10346.
18 J. D. Roy-Mayhew, D. J. Bozym, C. Punckt and I. A. Aksay, *ACS Nano*, 2010, **4**, 6203–6211.
19 Y. Xue, J. Liu, H. Chen, R. Wang, D. Li, J. Qu and L. Dai, *Angew. Chem. Int. Ed.*, 2012, **51**, 12124–12127.
20 S. Ito, S. M. Zakeeruddin, P. Comte, P. Liska, D. Kuang and M. Grätzel, *Nat. Photonics*, 2008, **2**, 693–698.
21 S. Ito, N.-L. Ha, G. Rothenberger, P. Liska, P. Comte, S. M. Zakeeruddin, P. Péchy, M. Khaja and M. Grätzel, *Chem. Commun.*, 2006, 4004–4006.
22 L. Hu, D. S. Hecht and G. Grüner, *Chem. Rev.*, 2010, **110**, 5790–5844.
23 F. Hao, P. Dong, J. Zhang, Y. Zhang, P. E. Loya, R. H. Hauge, J. Li, J. Lou and H. Lin, *Sci. Rep.*, 2012, ***2***, 368.
24 K. S. Lee, W. J. Lee, N.-G. Park, S. O. Kim and J. H. Park, *Chem. Commun.*, 2011, **47**, 4264–4266.
25 R. L. McCreery, *Chem. Rev.*, 2008, **108**, 2646–2687.
26 A. N. Patel, M. G. Collignon, M. A. O'Connell, W. O. Y. Hung, K. McKelvey, J. V. Macpherson and P. R. Unwin, *J. Am. Chem. Soc.*, 2012, *134*, 20117–20130.
27 A. Chou, T. Böcking, N. K. Singh and J. J. Gooding, *Chem. Commum.*, 2005, 842-844.
28 C. R. Bradbury, J. Zhao and D. J. Fermin, *J. Phys. Chem. C*, 2008, **112**, 10153–10160.
29 Z. Liu, Z. Shen, T. Zhu, S. Hou, L. Ying, Z. Shi and Z. Gu, *Langmuir*, 2000, **16**, 3569–3573.
30 J. J. Gooding, R. Wibowo, J. Liu, W. Yang, D. Losic, S. Orbons, F. J. Mearns, J. G. Shapter and D. B. Hibbert, *J. Am. Chem. Soc.*, 2003, **125**, 9006–9007.
31 T. Umeyama, H. Imahori, *Energy Environ. Sci.*, 2008, **1**, 120–133.
32 K. E. Moore, B. S. Flavel, A. V. Ellis and J. G. Shapter, *Carbon*, 2011, **49**, 2639–2647.
33 M. Bissett, A. Barlow, C. Shearer, J. Quinton and J. G. Shapter, *Carbon*, 2012, **50**, 2431–2441.

34 P. Diao, Z. Liu, B. Wu, X. Nan, J. Zhang and Z. Wei, *ChemPhysChem*, 2002, **10**, 898–901.
35 Md. A. Aziz, S. Patra and H. A. Yang, *Chem. Commun.*, 2008, 4607–4609.
36 A. J. Bard and L. R. Faulkner, *Electrochemical Methods: Fundamentals and Applications*, 2nd ed., Wiley, New York, **2000**, pp. 231–239.
37 D. J. Garrett, B. S. Flavel, J. G. Shapter, K. H. R. Baronian and A. J. Downard, *Langmuir*, 2010, **26**, 1848–1854.
38 M. S. Dresselhaus, G. Dresselhaus, R. Saito and A. Jorio, *Phys. Rep.*, 2005, **409**, 47–99.
39 J. Nelson, *The Physics of Solar Cells*, Imperial College Press, London, **2003**, pp. 11–13.
40 T. N. Murakami, N. Koumura, T. Uchiyama, Y. Uemura, K. Obuchi, N. Masaki, M. Kimura and S. Mori, *J. Mater. Chem. A*, 2013, **1**, 792–798.
41 S. Ahmad, T. Bessho, F. Kessler, E. Baranoff, J. Frey, C. Yi, M. Grätzel and Md. K. Nazeeruddin, *Phys. Chem. Chem. Phys.*, 2012, **14**, 10631–10639.
42 A. Hauch and A. Georg, *Electrochim. Acta*, 2001, **46**, 3457–3466.
43 D. Chattopadhyay, I. Galeska and F. Papadimitrakopoulos, *J. Am. Chem. Soc.*, 2001, **123**, 9451–9452.
44 F. Hao, P. Dong, Q. Luo, J. Li, J. Lou and H. Lin, *Energy Environ. Sci.*, 2013, **6**, 2003–2019.
45 L. Kavan, J.-H. Yum and M. Grätzel, *Nano Lett.*, 2012, **11**, 5501–5506.
46 X. Xu, D. Huang, K. Cao, M. Wang, S. M. Zakeeruddin and M. Grätzel, *Sci. Rep.*, 2013, **3**, 1489.
47 S. Peng, J. Liang, S. G. Mhaisalkar and S. Ramakrishna, *J. Mater. Chem.*, 2012, **22**, 5308–5311.